

Drivability enhancement and transient emission  
reduction for a mild hybrid diesel-electric truck

*Original*

Drivability enhancement and transient emission  
reduction for a mild hybrid diesel-electric truck / Galvagno, Enrico; Velardocchia, Mauro; Vigliani, Alessandro. - In:  
INTERNATIONAL JOURNAL OF POWERTRAINS. - ISSN 1742-4267. - STAMPA. - 2:2/3(2013), pp. 262-291.

*Availability:*

This version is available at: 11583/2503143 since:

*Publisher:*

Inderscience Enterprises Ltd.

*Published*

DOI:

*Terms of use:*

This article is made available under terms and conditions as specified in the corresponding bibliographic description in the repository

*Publisher copyright*

(Article begins on next page)

# Drivability enhancement and transient emission reduction for a mild hybrid diesel-electric truck

E. Galvagno, M. Velardocchia and A. Vigliani\*

Dipartimento di Ingegneria Meccanica e Aerospaziale  
Politecnico di Torino  
Corso Duca degli Abruzzi 24  
10129 Torino - Italy  
E-mail: [enrico.galvagno@polito.it](mailto:enrico.galvagno@polito.it)  
E-mail: [mauro.velardocchia@polito.it](mailto:mauro.velardocchia@polito.it)  
E-mail: [alessandro.vigliani@polito.it](mailto:alessandro.vigliani@polito.it)  
\*Corresponding author-2

**Keywords** hybrid vehicles; emission reduction; torsional oscillation damping; control allocation; drivability

**Abstract** *This paper deals with modelling and control methodologies applied to a heavy truck equipped with a parallel hybrid electric drivetrain. The actuator redundancy, typical of the mild-hybrid vehicle configuration, allows the powertrain control system to enhance the vehicle drivability, in terms of smooth driving and promptness, while reducing transient diesel engine emissions, in comparison with conventional pure thermal engine vehicles.*

*The electric motor, characterised by a high-bandwidth torque control, is here utilised not only to dampen the driveline oscillations that arise during rapid torque transients, e.g. when the driver accelerates the vehicle at full throttle in low gears, but also to keep the engine working with slow torque gradients, as required by transient emission reduction strategies.*

*The driveline is modelled by lumped parameters, considering also the damping effects of the tyres. A detailed nonlinear model is used as reference for the performance comparison of different simplified linear models. The best linear model is selected and used for the design of a LQR-based closed-loop controller aiming at reducing the driveline torsional vibrations. The regulation task (active vibration damping) is separated from the distribution task (torque splitting between the two motors).*

# 1 Introduction

Hybrid electric vehicles (HEVs), using an internal combustion engine (ICE) and electric motor-generators (EM), are becoming quite popular due to restrictions on exhaust gas emissions and fuel consumption; this trend will probably become more relevant in the next future.

A HEV can adjust the traction torque more quickly than conventional vehicles due to the presence of electric motors. As a result, the vehicle response to driver traction request can be very fast; unfortunately, these rapid torque changes also cause vibrations, which in turn degrade drivability. More specifically, vibrations in a mild-hybrid electric vehicle occur upon engine start/stop, a vibration unrelated to the driver's actions, or during rapid torque transients, e.g. when the driver suddenly accelerates (or decelerates) the vehicle, with the so called tip-in (or tip-out) manoeuvre.

Since drive comfort is an increasingly important issue when buying a vehicle, solutions to reduce the shuffle vibrations, related to the lowest torsional mode of the transmission, play an important role in the HEV control algorithm development.

The goal of this study is to reduce vibrations and transient diesel engine emissions due to rapid changes in driver demand by developing a suitable control of the electric and thermal actuators. [Hagena et al. \(2006\)](#) state that “an instantaneous load increase was found to produce peak NOx values 1.8 times higher and peak particulate concentrations an order of magnitude above levels corresponding to a five-second ramp-up. This result provides insight into relationship between driver aggressiveness and diesel emissions”.

The first step is to build a transmission model, able to describe the dynamic behaviour of the whole system: many different techniques can be used to this aim, as discussed by [Farshidianfar et al. \(2001\)](#) who face the problems related to the complexity of models, aiming at representing drivelines with increasing accuracy by using hybrid modelling techniques (DLMT).

One aspect that is often greatly simplified in drivetrain torsional models is the effect of the tyres, which are a relevant source of damping within the conventional powertrain. Therefore including a more accurate representation of tyres in powertrain models has relevant effects on the simulated dynamics.

The need of an appropriate model for the tyre behaviour has been widely discussed in the literature: [Rill \(2006\)](#) asserts that “the sufficient description of the interactions between tire and road is one of the most important tasks of vehicle modelling, because all the other components of the chassis influence the vehicle dynamic properties via the tire contact forces and torques”. [Rill \(2006\)](#) proposes to adopt relaxation lengths which include the wheel load and slip dependencies, automatically generated from the steady state tire properties.

[Guzzomi et al. \(2010\)](#) present the results of identification techniques aimed at describing the tyre torsional vibrational dynamics: they found that over the frequency range tested (10-50 Hz), the damping is more accurately represented as hysteretic and not viscous when lightly loaded. Their results indicate that the viscous or hysteretic damping assumption has significant effects on the predicted frequency response of the powertrain.

Other authors ([Bartram et al., 2008](#)) describe three tyre models: a simple torsional spring model, a linear slip model and a fixed relaxation length-based model. In the latter two models, nonlinearity is introduced via the implementation of the instantaneous slip ratio, which represents a nonlinear function of two of the state variables: the rotational speed of the wheels and the forward speed of the vehicle. Ultimately, through appropriate linearisation, all three models are suitable for linear state-space analysis, thus enabling to estimate the transmission natural frequencies and modal shapes.

Moreover two more accurate nonlinear models, i.e. a fully non-linear relaxation length model ([Pacejka, 2002](#)) and a tyre model that takes into account the inertia of the tyre belt, have been presented and compared. [Bartram et al. \(2008\)](#) state that belt model appears to be the most appropriate for use in driveline studies, not because of its frequency content, but due to the relatively significant differences predicted in terms of response amplitude caused by belt inertia.

[Canudas-de-Wit et al. \(2003\)](#) present a new dynamic friction tyre model, based on the LuGre model, able to capture accurately the transient behaviour of the friction force observed during

transitions between braking and acceleration. Automotive applications are presented by [Dolcini et al. \(2010\)](#), who modelled the link between wheels and vehicle mass through a lumped LuGre tire ground contact model.

This paper deals with a parallel hybrid architecture used on a heavy commercial truck, similar to the one proposed by [Fredriksson \(2006\)](#). He presents a driveline model and a powertrain control aimed at actively damp out driveline oscillations by using the internal combustion engine in combination with the electric machine. With regard to the linear model used for the model-based control design, this research proposes a more accurate tyre model, i.e. a ‘fixed relaxation length model’ like the one proposed by [Bartram et al. \(2008\)](#), hence decoupling the kinematic behaviour of the driving rear tyres from free rolling condition. This model belongs to the category of point contact transient tyre models and is based on the combination of a steady-state slip-based force function that accepts a transient state, the so called transient slip quantity, as an input. The steady-state force function is here a linearisation of the Pacejka’s magic formula model.

All the controllers are tested on a non linear vehicle model considering a fully non-linear relaxation length tyre model. The nonlinear model is used as reference for the performance comparison of different simplified linear models.

Researchers have faced the problem of reducing driveline vibrations with different techniques. [Ito et al. \(2007\)](#) present a vibration-reducing control method for the motor-generators in hybrid vehicles, by means of two types of controllers. The first reduces the vibrations due to engine torque ripple at engine start, while the second reduces the drivetrain vibrations: the effectiveness of these controllers in reducing vibration is confirmed experimentally.

[Berriri et al. \(2008\)](#) deal with the problem of active damping of driveline oscillations in order to improve drivability and passenger comfort. They present a robust and efficient controller, driving the engine in order to actively damp the driveline oscillations. Their methodology is based on the prediction and compensation of the shaft torque at relevant frequencies. It leads to a controller having only a few tuning parameters, with a clear meaning, that can be adjusted directly on the vehicle.

The objective of [Baumann et al. \(2006\)](#) is to present a model-based control concept that prevents the driveline from oscillating, a so-called anti-jerk control. The predictive controller is designed with the help of the root locus technique and is evaluated on a test car with a diesel engine.

Another improvement with respect to the work of [Fredriksson \(2006\)](#), is the introduction of three control systems: the first one is devoted to the direct vehicle acceleration control, the second consists in a classical torque control with a superposed active damping of the oscillation whereas the third is a vehicle speed control. The torque distribution between the actuators is managed as a separate task from the regulation task (oscillation damping), using a specific control allocation algorithm that does not need the solution of an optimisation problem.

Using the proposed control method the following results can be obtained:

- the diesel engine can deliver a slow varying torque, thus satisfying the rate limitation required to reduce the transient emissions (see ? and [Auerbach et al. \(2011\)](#));
- the diesel engine supplies the steady state value required by the driver;
- the electric motor covers the high dynamic torque transients requested by the active oscillation controller;
- the combination of the torque from the two actuators guarantees a good level of comfort even in saturation conditions, without adversely affecting the responsiveness of the vehicle.

## 2 The Hybrid Electric Vehicle (HEV) architecture

This paper is focused on modelling and control of a mild hybrid rear-wheel drive truck (Fig. 1). Such hybrid architecture, also referred to as Belted Alternator Starter (BAS) system, is composed of two actuators: a reversible electric machine, that can act as both motor and generator, and a conventional Diesel engine. These motors are mechanically coupled through a belt transmission

in a parallel hybrid configuration.

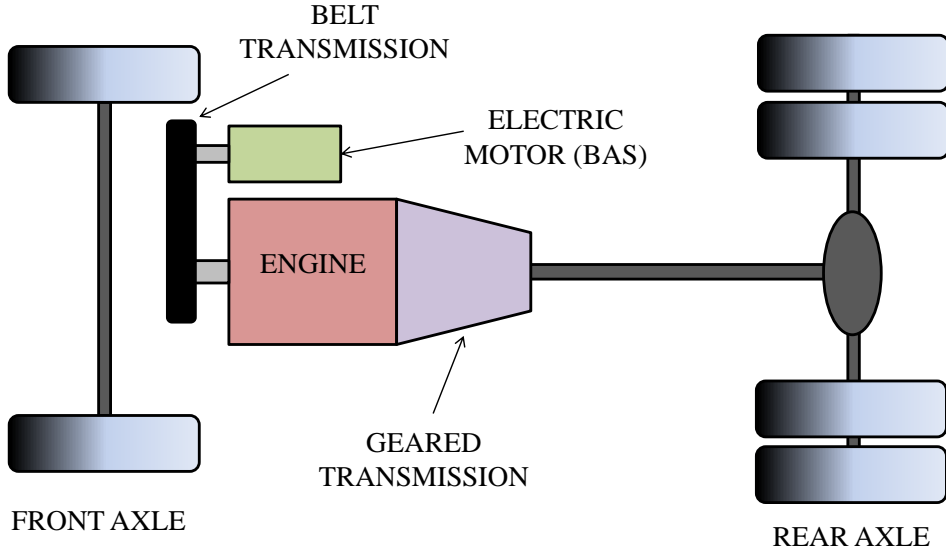


**Figure 1:** truck hybrid transmission scheme

The electric motor within this layout can not propel the vehicle by itself, but behaves mainly as a power booster, i.e. it assists the engine when extra power is demanded.

This propulsion system architecture allows an efficient engine start and stop functionality and the storage of part of braking energy in the battery for future usage.

In addition to the former well known features, it must be noted that the high bandwidth typical of the electric machine torque control can be proficiently used to balance the much slower response of the internal combustion engine. There are basically two reasons why the internal combustion engine should be considered, from a control-oriented point of view, a rate limited torque actuator: firstly because of its physical working principle, that involves a speed dependent combustion delay and, in case of turbocharged engine, also a turbo-lag ([Koprubasi \(2008\)](#) discusses simplified models for both these phenomena); secondly because of the engine emission control strategy that may smooth the high rate of load changes with the aim of minimising the emission formation (NOx and soot).

In conclusion, since a considerable amount of emission can be attributed to the dynamic torque changes, the operation of the internal combustion engine at reduced dynamics, called phlegmatization ([Auerbach et al., 2011](#)), in combination with a highly dynamic electric motor able to cover the impulsive torque requests, constitutes an effective way to establish a trade-off between emissions and dynamic performance.

## 2.1 Dynamic models

Three dynamic models of the same hybrid electric vehicle have been implemented. The most complex *nonlinear model* (NLM) will be considered as the reference to test the accuracy of the other simplified linearised models and will be utilised also to test the control algorithms. It includes nonlinear elastic and damping behaviour of the torsional damper, half shafts linear elastic characteristic, transient fully nonlinear model proposed by [Pacejka \(2002\)](#) for the tyres, the vehicle longitudinal dynamics (one degree of freedom) and longitudinal load transfer computation.

The *five-state linearised model* (SS5) differs from the previous model in neglecting the effects of torsional damper and longitudinal load transfer.

Finally, the *three-state linearised model* (SS3) further reduces the number of degrees of freedom introducing the hypothesis of pure rolling motion for all the tyres.

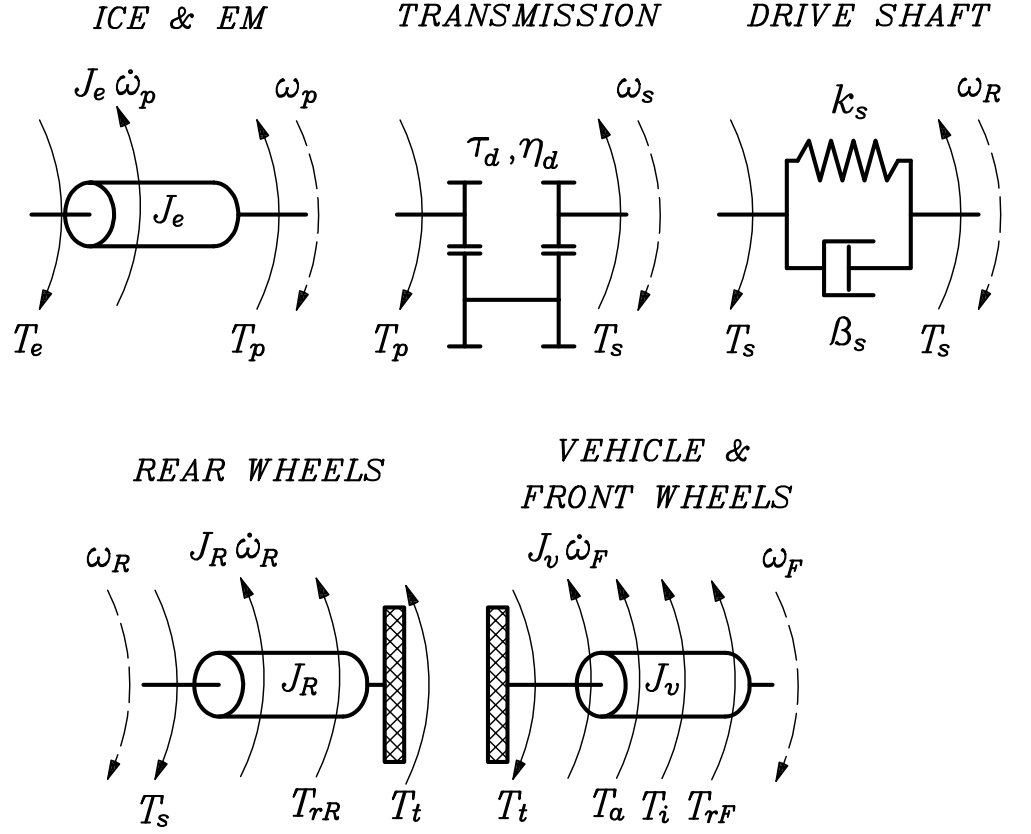


**Figure 2:** free body diagrams of the analysed vehicle

## 2.2 Dynamic equations

The free body diagrams of the main driveline components are reported in Fig. 2. Considering a unitary efficiency for the belt transmission, both the internal combustion engine and the electric motor can be modelled with an equivalent mass moment of inertia  $J_e$

$$J_e = J_{ICE} + J_{EM}\tau_b^2 \quad (1)$$

and a total driving torque  $T_e$

$$T_e = T_{ICE} + \tau_b T_{EM}. \quad (2)$$

At the gearbox primary shaft the torque equilibrium equation is

$$T_e - T_p = J_e \ddot{\vartheta}_p. \quad (3)$$

The speed reductions and the power losses due to the transmission and drive axle are described by the kinematic equation

$$\dot{\vartheta}_p = \tau_d \dot{\vartheta}_s \quad (4)$$

and by the torque relation

$$T_s = \eta_d \tau_d T_p. \quad (5)$$

The elasticity of the whole driveline is lumped using a torsional spring and viscous damper element, whose equation is

$$T_s = k_s(\vartheta_s - \vartheta_R) + \beta_s(\dot{\vartheta}_s - \dot{\vartheta}_R). \quad (6)$$

Since the wheels of the dead axle, i.e. the front axle, are supposed to be in rolling condition, the inertial effect of both the vehicle and the front wheels can be described through an equivalent mass moment of inertia  $J_v$  evaluated at the front wheel shaft:

$$J_v = M_v R_w^2 + J_F. \quad (7)$$

The vehicle longitudinal dynamic equilibrium gives:

$$T_t - J_v \ddot{\vartheta}_F - T_a - T_i - T_{rF} = 0, \quad (8)$$

where the torque due to road longitudinal inclination  $\alpha$  is

$$T_i = N_i R_w = Mg \sin \alpha R_w \quad (9)$$

and the equivalent aerodynamic resistance is

$$T_a = N_a R_w = \frac{1}{2} \rho S_v D R_w v^2, \quad (10)$$

where the vehicle speed is computed as

$$V = \dot{\vartheta}_F R_w \quad (11)$$

since slip is assumed to be null for the front tyres.

A first relevant difference with the existing models (Ito et al., 2007; Fredriksson, 2006) is here introduced, removing the ideal hypothesis of free rolling motion for the driving axle and modelling the dynamic effects of the rear drive tyres by introducing the longitudinal slip

$$\sigma = 1 - \frac{\dot{\vartheta}_F}{\dot{\vartheta}_R} = \frac{\dot{\vartheta}_R - \dot{\vartheta}_F}{\dot{\vartheta}_R}. \quad (12)$$

This assumption results in an additional degree of freedom for the system, correspondent to the wheel rotation  $\vartheta_R$ ; consequently it is necessary to write a dynamic equilibrium equation for the rear driving axle:

$$T_s - T_t - J_R \ddot{\vartheta}_R - T_{rR} = 0, \quad (13)$$

where  $T_t$  is the torque generated by the longitudinal force of the rear tyres.

The rolling resistance torques for the front and rear axles increase quadratically with the rotational speed of the wheels:

$$T_{rF} = \gamma N_z R_w (f + K \dot{\vartheta}_F^2) \quad (14)$$

$$T_{rR} = (1 - \gamma) N_z R_w (f + K \dot{\vartheta}_R^2) \quad (15)$$

where  $N_z = Mg \cos \alpha$  is the total load normal to ground.

Moreover, with reference to the tyres behaviour, the proposed model takes into account the tyre relaxation length, which models the delayed response of the tyre with respect to applied driving or braking action. Also this hypothesis results in an additional differential equation, i.e.,

$$\dot{T}_t \delta + T_t = \tilde{T}_t, \quad (16)$$

where

$$\delta = \frac{L_t}{\dot{\vartheta}_F R_w} \quad (17)$$

is the time constant due to the tyre relaxation length  $L_t$ .

Since this time constant is inversely proportional to a state variable  $\dot{\vartheta}_F$ , in order to avoid a nonlinearity in the system equations, the front wheel speed in eq.(17) is replaced by its initial condition  $\dot{\vartheta}_{F,0} = V_0/R_w$ , the same used for the system linearisation. Furthermore, the value of the relaxation length, although some authors (Rill, 2006) showed its dependence on normal load and longitudinal slip, is here considered constant in order to obtain a linear system.

The steady state value of the tyre torque can be determined as

$$\tilde{T}_t = N_x R_w = C_t \sigma R_w = C_t R_w \frac{\dot{\vartheta}_R - \dot{\vartheta}_F}{\dot{\vartheta}_R}, \quad (18)$$

where the longitudinal slip stiffness  $C_t$  can be estimated from the linearisation of the steady state characteristic of longitudinal force  $N_x$  vs. longitudinal slip  $\sigma$  curve for a given vertical load (supposed constant). In eq.(18), the relation between force and slip is considered linear; obviously such approximation is valid only for small values of slip (less than 10% in high adherence conditions, even less on low grip surfaces).

In order to apply control techniques, it is useful to write the equations in the state space; hence these equations need to be linearised in the neighbourhood of an equilibrium point.

The state space description of the dynamic system is

$$\{\dot{x}\} = [A]\{x\} + [B]\{u\} + [H]. \quad (19)$$

The linearisation process and the final matrices are reported in Appendix B.

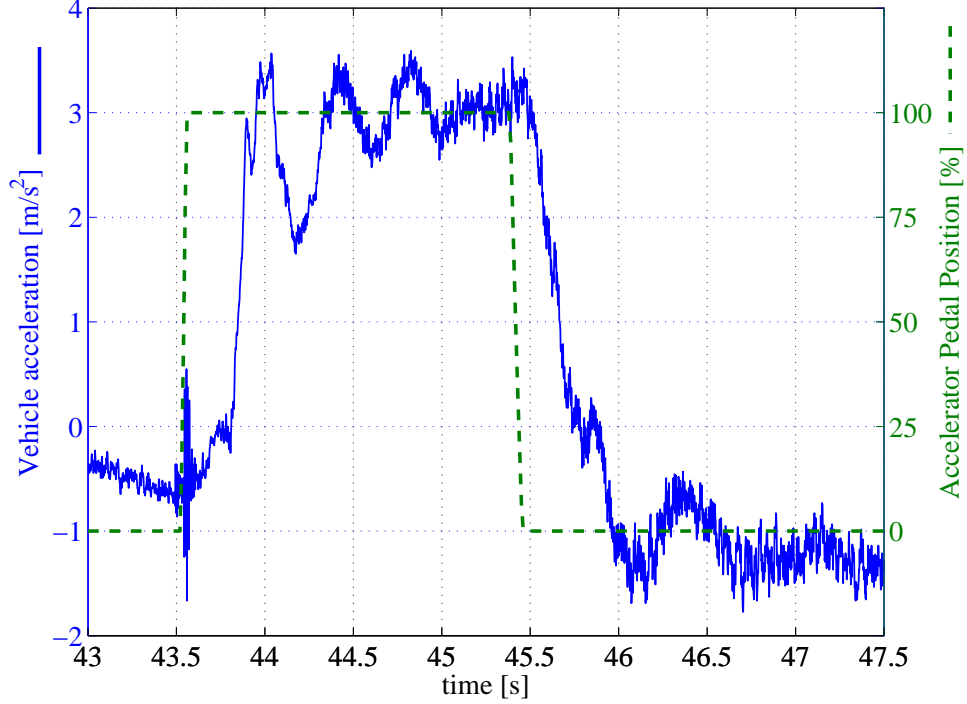


**Figure 3:** accelerator pedal position and vehicle acceleration measured during a tip-in/tip-out experimental test on a passenger car

### 3 Tip-in open loop response

The vehicle longitudinal acceleration signal recorded during a torque tip-in/tip-out test, see e.g. Fig. 3, is often used to evaluate the drivability of conventional cars. In fact, some important aspects related to driver subjective impressions can be highlighted, such as the promptness of the powertrain control system to accomplish sudden changes of the vehicle acceleration and the drive smoothness requiring extremely small oscillations during transients.

Consequently, during open-loop simulations the selected input for the dynamic system is the total torque  $T_e$ , delivered at the transmission input shaft by the two motors, while the monitored variable is the vehicle longitudinal acceleration.

The input torque follows a step change at 1.5 s from 0 to 200 Nm in 4<sup>th</sup> gear starting from a vehicle speed of 5 km/h.

This section is organised as follows. First of all, in section 3.1, we identify the linear model with the lowest possible number of states capable of reproducing, with an acceptable accuracy, the open loop response of the non linear model used as benchmark. Then, in section 3.2, a rate limited step response is analysed with the aim of visualising the effect of the engine torque slope on the drivability of a pure thermal vehicle.

#### 3.1 Linearised models

The open-loop response for all the three models introduced in section 2.1 is shown in Fig. 4. To validate the results, the nonlinear model is considered as the reference model. From the comparison it appears that:

- the linearisation in model SS5 gives excellent results in the neighbourhood of the equilibrium configuration used for linearising the system;
- the free rolling hypothesis adopted in model SS3 overestimates the natural frequency and underestimates the damping; hence an additional damping accounting for the tyre dissipation is required to match the system response at least in terms of damping ( $\beta_s = 3000$  Nms/rad for SS3 model,  $\beta_s = 0$  Nms/rad for all the other models).

Figure 5 compares the values of the wheel slip between the nonlinear and the linearised SS5 model, while obviously the slip in SS3 is constantly null, in accordance with the hypothesis of pure



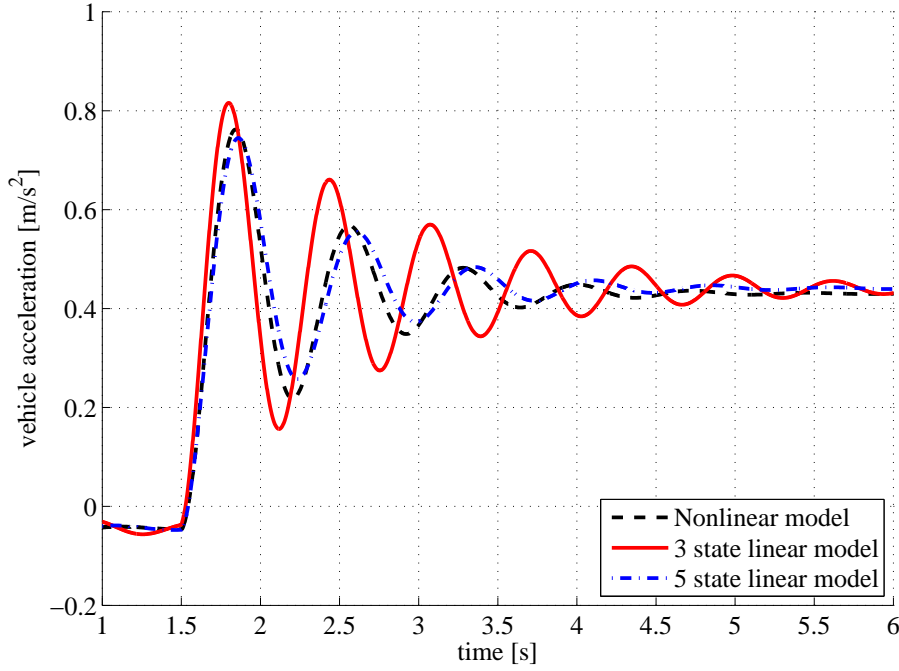


**Figure 4:** comparison of the open-loop step response for the three analysed models

rolling motion. There is a relevant difference in the initial overshoot since the linearised model overestimates of about 100% the slip computed by the nonlinear model; conversely the amplitude of the following oscillations becomes progressively better described. For larger simulation time, the system drifts from the initial condition (e.g., the vehicle speed increases) and consequently the difference between the models grows, especially in terms of steady state value.

These results prove that it is necessary to increase the model complexity, by introducing two additional state variables (both for the tyre model) to the basic 3 state linear model, in order to characterise the vehicle behaviour during the tip-in manoeuvre.

### 3.2 Torque slope sensitivity

The operation of the internal combustion engine at reduced dynamics is a method to reduce the emissions due to high rates of load change (Auerbach et al., 2011). It is therefore interesting to understand the effect that different rising (or falling) torque slopes have on the open-loop system dynamics and hence on the drivability. With reference to Fig.6 and Fig.7, increasing the slope values from 150 Nm/s to 600 Nm/s causes larger oscillation amplitude of the vehicle acceleration, while the rising time reduces progressively. An optimal drivability calibration in this case is 300 Nm/s: the acceleration quickly increases and reaches the steady state value with small oscillations.

## 4 The closed-loop control systems

Two closed-loop control schemes are analysed, as visible in Fig.8. The first one, named (A) in Fig.8, allows to directly control the vehicle acceleration, which is, as already mentioned, one of the most important quantities to be monitored for drivability assessment. During the tuning process of the control algorithm, several constraints can be applied to its time evolution according to the desired compromise between promptness and smooth driving.

The second scheme (B) consists of a driver torque control with active damping of the drivetrain oscillations. In practical terms, the torque requested from the driver  $T_{dr}$  is computed based on the accelerator pedal map (which correlates the engine torque set-point to the engine speed and to the accelerator pedal position) and is then converted into a vehicle longitudinal acceleration request  $a_{x,ref}$  through a simplified 1 d.o.f. vehicle model. Consequently also the second scheme can be brought back to the first one.

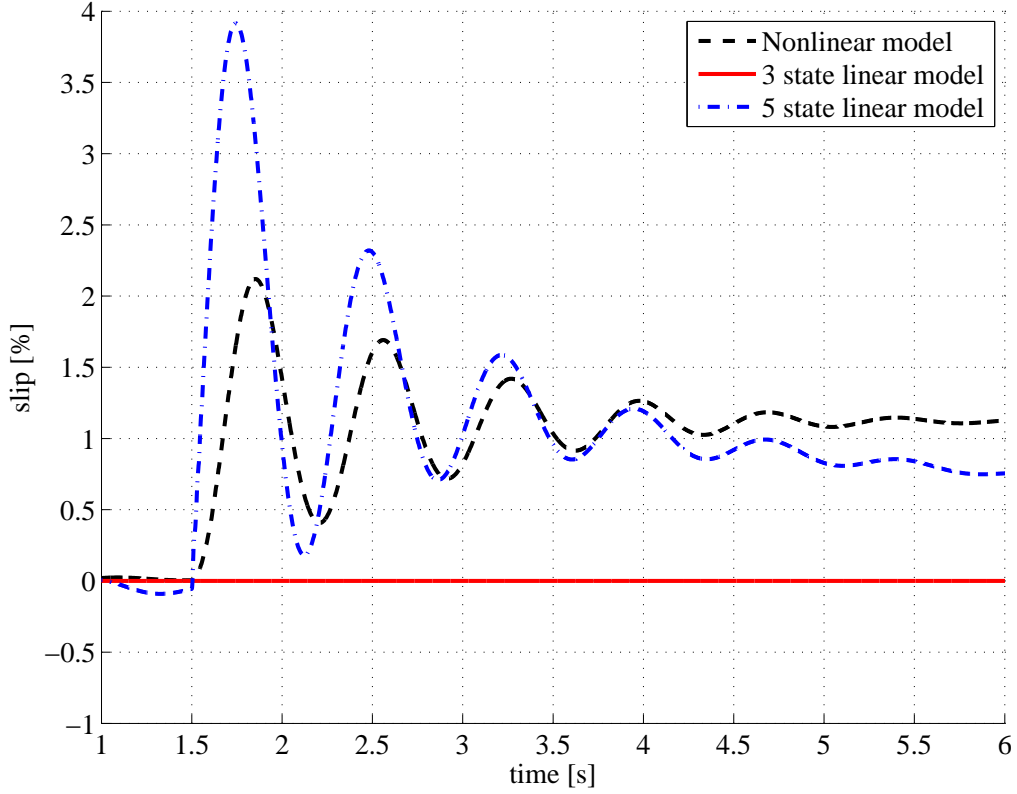


**Figure 5:** comparison between the longitudinal slip of the drive wheels of the three models during a tip-in test

The following elements of the control systems are therefore common for the two approaches and will be described together. The acceleration demand is converted by integration into a reference speed for the wheels in free rolling  $\omega_{F,ref.}$ ; in this way, the condition on the vehicle longitudinal acceleration becomes a specification for one of the state variables ( $\omega_F$ ).

#### 4.1 Measures and state estimation

The measured outputs  $y$  are the engine angular speed and the front wheel velocities, which are commonly available on the vehicle Controller Area Network (CAN), shared by the engine and brake nodes respectively. The delay attributable to the working principle of these sensors is modelled by means of a variable time delay  $\delta_s$ , depending on the angular speed  $\omega$  and on the number of pulses per revolution  $z_s$ :

$$\omega_{meas}(t) = \omega(t - \delta_s) = \omega \left( t - \frac{\pi}{z_s \omega_F} \right) \quad (20)$$

To achieve the closed loop control with a full state feedback, the states that cannot be measured are estimated by a Kalman filter, which gives the estimated state vector  $\hat{x}$  based on the inputs  $u$  and on the measured outputs  $y$ , see Fig.8.

#### 4.2 Control design method

The solution of the control problem has been subdivided into two tasks: the first one is to design a control law determining the total control effort  $v$ , while the second task is to distribute the total control demand among the actuators, as suggested by Fredriksson (2006).

##### The equivalent SI system

The original two-input ( $T_{ICE}$  and  $T_{EM}$ ) system described by eq.(19) can be converted in the following equivalent single-input (SI) system:

$$\{\dot{x}\} = [A]\{x\} + [B_1]v + [H] \quad (21)$$

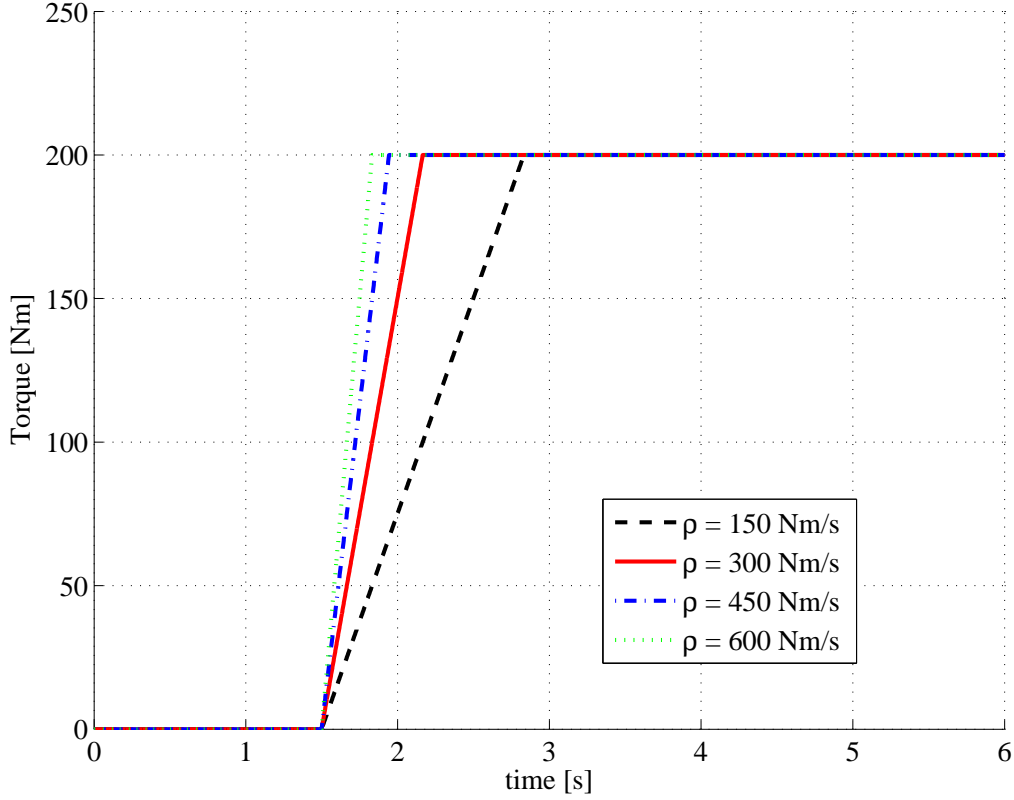


**Figure 6:** input torque during the engine torque slope sensitivity analysis

where  $[B_1]$  is a  $5 \times 1$  matrix such that  $[B] = [B_1][B_2]$  and  $v = [B_2]\{u\}$ , and  $v$  is the equivalent input signal ( $T_e$ ).

The factorisation of B gives:

$$[B_1] = \begin{bmatrix} 0 \\ 0 \\ \frac{1}{J_e} \\ 0 \\ 0 \end{bmatrix}; \quad [B_2] = \begin{bmatrix} 1 & \tau_b \end{bmatrix}. \quad (22)$$

The adopted control law is

$$v = K_{ff}\omega_{F,ref} - [K] \{\hat{x}\} \quad (23)$$

where the goal of the feed-forward part ( $K_{ff}\omega_{F,ref}$ ) is to make the controlled state  $\omega_F (= x_4)$  coincident with the reference value  $\omega_{F,ref}$  when the transient is over ( $\dot{x} = 0$ ), as demonstrated in the following passages.

In steady state conditions and neglecting the  $[H]$  matrix, the state equation (21) becomes

$$[A]\{x\} = -[B_1]\{v\}. \quad (24)$$

Imposing that the steady state value is equal to the reference value, it holds:

$$\omega_{F,ref} = \omega_F = [C_F]\{x\} = [00010] \{x\}, \quad (25)$$

where  $[C_F]$  is the vector that allows to select the state variable to be controlled (all zeros except for state 4, i.e.,  $\omega_F$ ).

By combining eq.(23),(24) and (25), the feedforward gain  $K_{ff}$  results:

$$K_{ff} = \left[ [C_F] \left( [B_1][K] - [A] \right)^{-1} [B_1] \right]^{-1} \quad (26)$$

To obtain the state feedback gain matrix  $[K]$ , which delineates the dynamic performance of the closed-loop control system, it is possible to adopt a full state feedback control design method, such

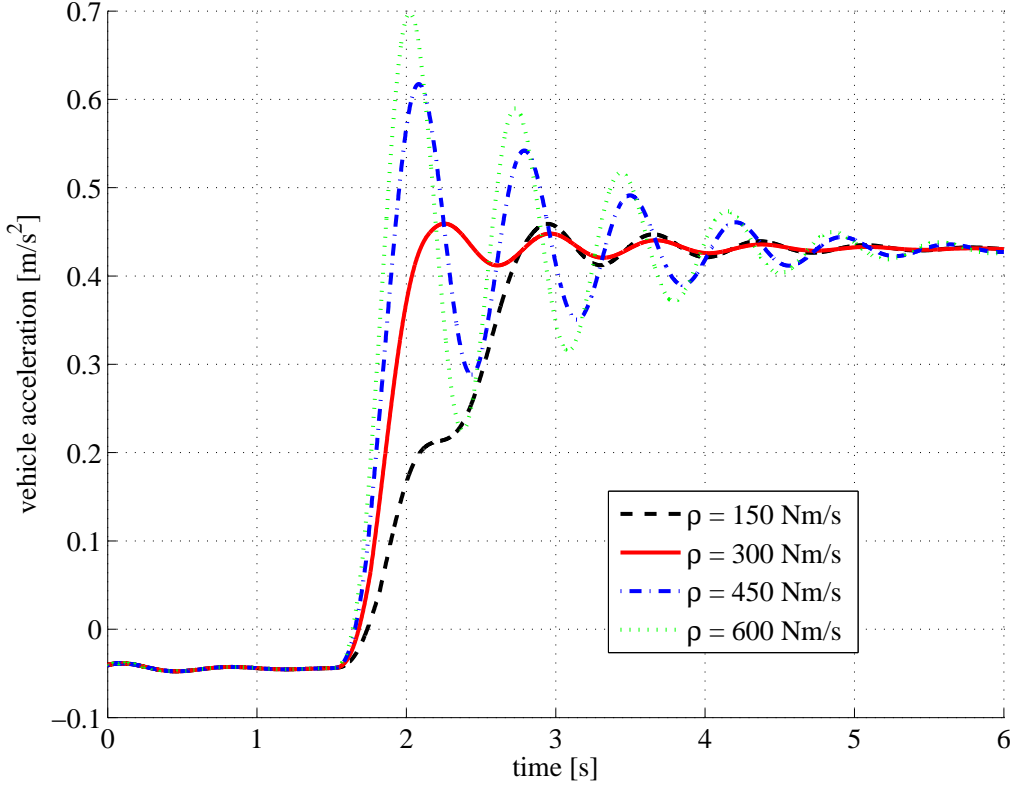


**Figure 7:** vehicle acceleration during engine torque slope sensitivity analysis

as the Linear Quadratic Regulator (LQR) design (Anderson and Moore, 1990), here proposed, rather than the pole placement method. The linearised optimal quadratic control grants that the closed loop linearised system is asymptotically stable and that the quadratic performance functional  $J([K])$  is minimised:

$$J([K]) = \int_0^\infty \left( \{x\}^T(t)[R_1]\{x(t)\} + \{u(t)\}^T[R_2]\{u(t)\} \right) dt. \quad (27)$$

The feedback matrix  $[K]$  can be obtained by solving the *Riccati equation* associated with the LQR problem:

$$[A]^T[P] + [P][A] - [P][B][R_2]^{-1}[B]^T[P] + [R_1] = 0; \quad (28)$$

$[K]$  is computed from  $[P]$ , which is the solution of equation (28), as

$$[K] = [R_2]^{-1}[B]^T[P]. \quad (29)$$

### The control allocation

Recall that the torque  $T_e$  applied at the transmission input shaft can be delivered by one of the two motors or by a combination of the two, see eq.(2) and that the control objective is to track the desired vehicle acceleration profile; then it follows that the analysed control system is over-actuated ( $[B]$  is rank deficient). Consequently, the control system has an additional degree of freedom that is used to split the total effort  $v$  between the internal combustion engine torque and the electric motor torque according to different criteria.

The easiest way to distribute such torque, also considering the low level of hybridisation typical of the considered BAS architecture, is to use the electric motor only to compensate for the dynamic limits of the engine.

Hence, a possible solution is described in the block diagram of Fig.9. The total torque  $v$  enters into a saturation block that bounds the range of the input signal to upper and lower saturation values deriving from the engine steady state maximum and minimum torque maps; then a rate limiter block is used to model the maximum rising and falling rate of the torque delivered by the engine. The EM torque is therefore the difference between the total torque requested by the controller  $v$  and the torque actually delivered by the engine  $T_{ICE}$ ; obviously also the EM torque

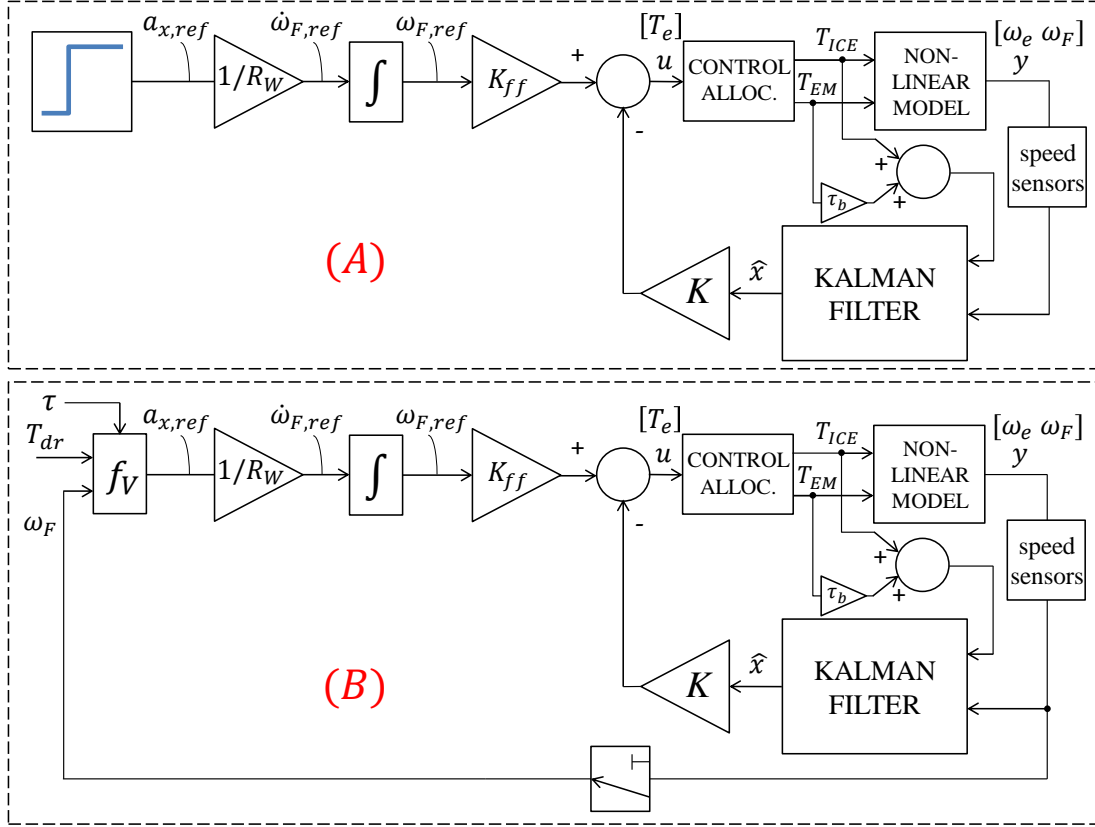


**Figure 8:** block diagrams of the two closed-loop control systems: (A) vehicle acceleration control; (B) driver torque control with active damping of drivetrain oscillations

is limited by the electric motor maximum and minimum values and rate limited according to the bandwidth ( $\approx 100$  Hz) of the electric motor torque control.

### The controller tuning procedure

To obtain the desired system performance, it is necessary to tune the two design matrices  $[R_1]$  and  $[R_2]$  of the cost functional  $J$ : they contain the penalties for the system states and control signal respectively, i.e.,  $[R_1]$  penalises the departure of system states from equilibrium while  $[R_2]$  intervenes on the energy of the control input. Matrix  $[R_2]$  is tuned based on the actuation system size and dynamics, while  $[R_1]$  is tuned based on the acceptable oscillations of the system states. In the examined case, the state closer to the vehicle acceleration is the torque acting on the driving wheels, i.e.,  $x_5 = T_t$ . Hence a first penalty will be placed on the main diagonal in position (5,5) in order to reduce the torque oscillations and consequently the vehicle longitudinal acceleration (note that the dynamics of the resistant loads is much slower and can be considered constant in first approximation, especially at low speed). Also term (4,4) is set different from zero, in order to control the acceleration integral, proportional to the velocity  $\omega_F$ .

Finally, it is advisable to set also term (2,2) different from zero, e.g. equal to (4,4), in order to reduce the speed difference between the free rolling and driving wheels: in other words, it is a way to contain the energy of the drive axle slip signal. A reasonable compromise can be achieved using the following values for the matrices:

$$[R_1] = \text{diag}(0, 1, 0, 1, 10^{-9}); \quad [R_2] = 10^{-6} \quad (30)$$

### 4.3 Influence of the truck model on the control performance

In section 3.1 we compared the open-loop response of the three models and we demonstrated the necessity to use the SS5 linear model to simulate the HEV. Here we want to analyse the role of the additional two states (respect to the basic SS3) in terms of control performance.

For this purpose, the nonlinear model is controlled by:

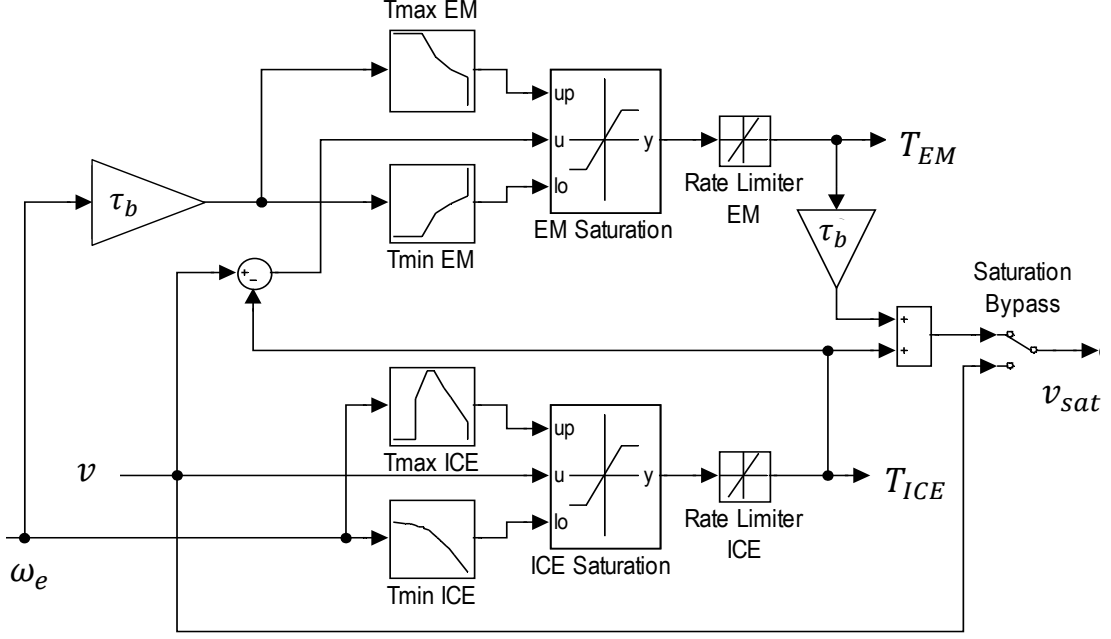


**Figure 9:** total control effort distribution between the actuators using the electric motor to compensate for the dynamic limits of the engine

- a 3 state controller, based on LQR design method applied to model SS3, with a 3 state observer, tuned on the same model;
- a 5 state controller, based on LQR design method applied to model SS5, with a 5 state observer, tuned on the same model.

The results shown in Fig.10 and 11 allow to state that the relevant differences highlighted in open loop are less evident in closed loop. The three state controller is able to provide the required performance for the closed loop control system and, moreover, the calibration made on the SS3 linear model can be extended to control the nonlinear model with a fairly accurate approximation of the achievable response.

Different control calibrations can reduce the rise time but cannot eliminate the acceleration steady-state error. However, it is of interest remarking that is not very important to accurately match the acceleration reference value, since this is only an estimate of what the vehicle is able to achieve for a given engine torque, and does not represent a direct specification of the driver, see Fig.8 (B). Consequently, it was not considered necessary to vary the control scheme aiming at annihilate the steady state error on the acceleration.

This difference is due to the system nonlinearities (it disappears when controlling the linearised models), mainly dependent on the tyre behaviour and on the motion resistances (proportional to the squared vehicle speed).

However this inaccuracy is relatively small and does not significantly affect the control performances. In fact, the proposed control architecture is able to satisfy the driver's requests and to actively damp the torsional oscillations.

#### 4.4 Vehicle acceleration closed-loop control

With reference to Fig.8(A), a vehicle acceleration set point profile can be translated into a speed profile for the front wheels in free rolling conditions:

$$\omega_{F,ref}(t) = \frac{1}{R_w} \left( \int_0^t a_{x,ref}(t) dt + V_0 \right). \quad (31)$$

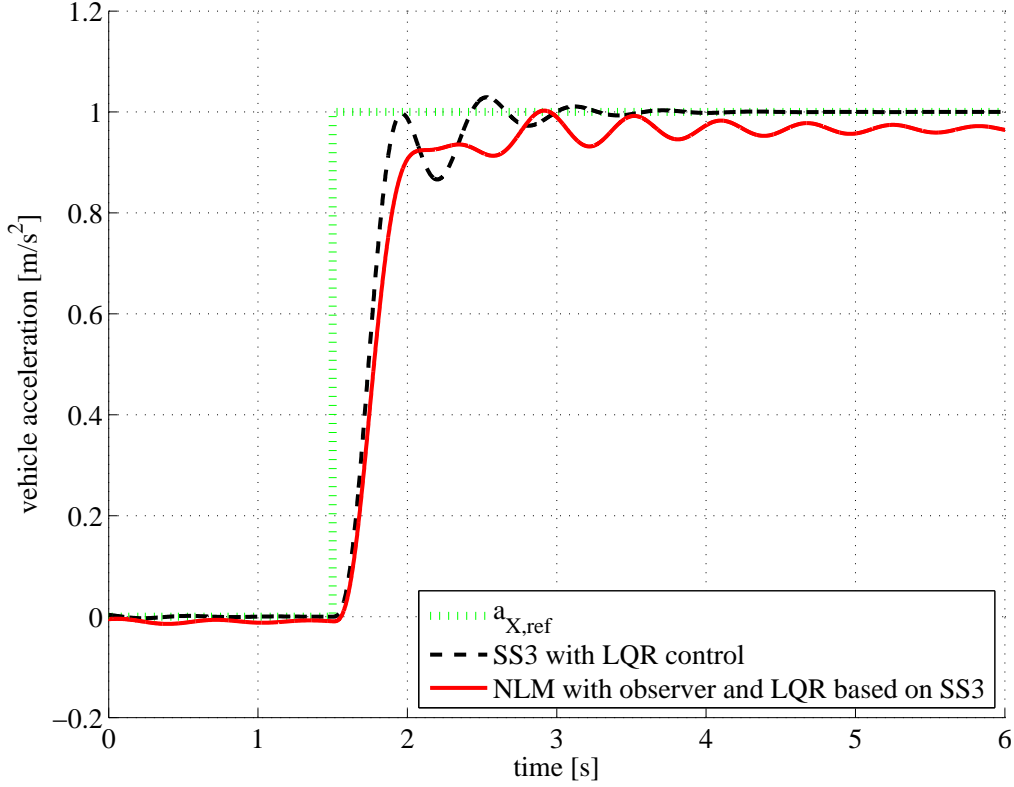


**Figure 10:** closed loop control of vehicle acceleration: step response of linear (SS3) and nonlinear model (NLM) with 3 state controller

### ‘Engine only’ operating mode

The engine only operational mode is here analysed: the EM intervention is inhibited and the vehicle is propelled only by means of the internal combustion engine.

The 5-state linear closed-loop controller has been applied to the non linear model, considering the physical characteristics of the engine, i.e. torque maps and rate limited torque response, in order to evaluate their effects on the dynamic performance. More specifically, this section discusses the impact of:

- the maximum engine torque slope (Fig.12)
- the calibration of the feedback gain matrix (Fig.13)

on the control performance.

With reference to Fig.12, the response optimisation of the control algorithm, based on the modification of the feedback gain matrix using LQR method, has been applied considering no limits on the control signal dynamics (ideal torque actuator with infinite torque slope capability,  $[R_2] = 10^{-6}$ ). Consequently, the faster is the engine dynamics the better is the response, that tends to the ideal calibration condition for  $s_{ICE} \rightarrow \infty$ . From these simulation results, it is evident that it would be better to adapt the control calibration to the real performance of the actuator.

For this purpose, Fig.13 shows how to set the controller design parameters to meet the maximum torque gradient (200 Nm/s in this case) that the engine can achieve, due for example to the intervention of a transient emission reduction strategy. Increasing  $[R_2]$  results in an energy reduction of the control signal: the response becomes weaker and the amplitude of the acceleration oscillations decreases. Moreover, if the rise time is not a critical design constraint, a simple first order low-pass filter can be applied on the engine torque to obtain a slow but smooth vehicle acceleration profile (see e.g. curves obtained with  $[R_2] = 2 \cdot 10^{-5}$  and  $[R_2] = 4 \cdot 10^{-5}$ ).

### ‘Hybrid’ operating mode

In the former paragraph it was shown that in case of an acceleration step, the method to reduce oscillations using a low dynamic torque actuator consists essentially in a low-pass filter to be

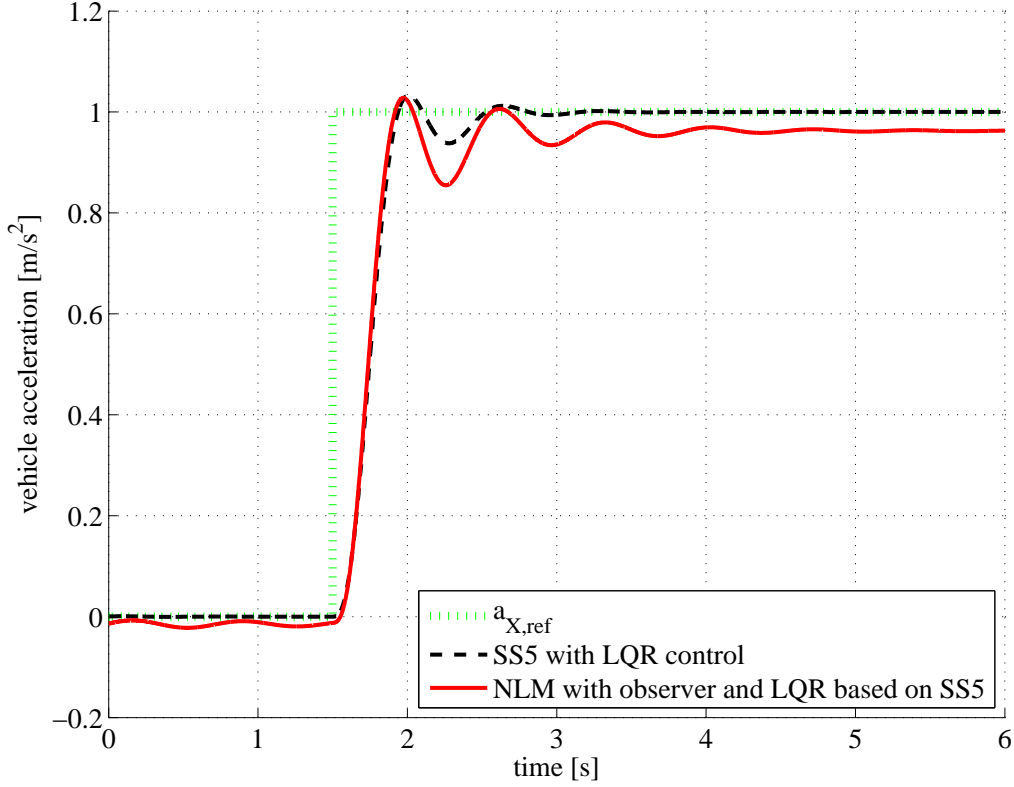


**Figure 11:** closed loop control of vehicle acceleration: step response of linear (SS5) and nonlinear model (NLM) with 5 state controller

applied to the driving torque. Here it will be proved that, to increase the promptness of the vehicle response and concurrently damp the torsional vibrations, a high dynamic electric motor can be used in combination with the thermal engine.

The actuator redundancy, typical of the considered hybrid powertrain scheme, allows the electric motor, within its saturation limits, to completely overcome the dynamic limit of the IC engine and to cope the ideal performance achievable with the considered driveline, as can be seen in Fig.14.

Irrespective of the value assumed by the torque slope, all the curves in Fig.14 are superimposed, i.e. the electric motor is able to actively compensate the vibrations. Different torque slopes evidently imply a different torque distribution between the motors (see Fig.15), i.e. the reduction of the maximum engine torque gradient involves an increase of the electric motor contribution, while maintaining the same total torque and consequently the same dynamic system response.

Finally, it is of interest underlining that the electric motor works only during transients, for a short time; hence it does not require too much energy from the energy storage system. The power ratio between the thermal engine and the electric motor can be about 10:1. In the simulations the electric motor rated power is  $\approx 30\text{kW}$ , while the diesel engine maximum power is  $\approx 330\text{kW}$  (data from Fredriksson (2006)).

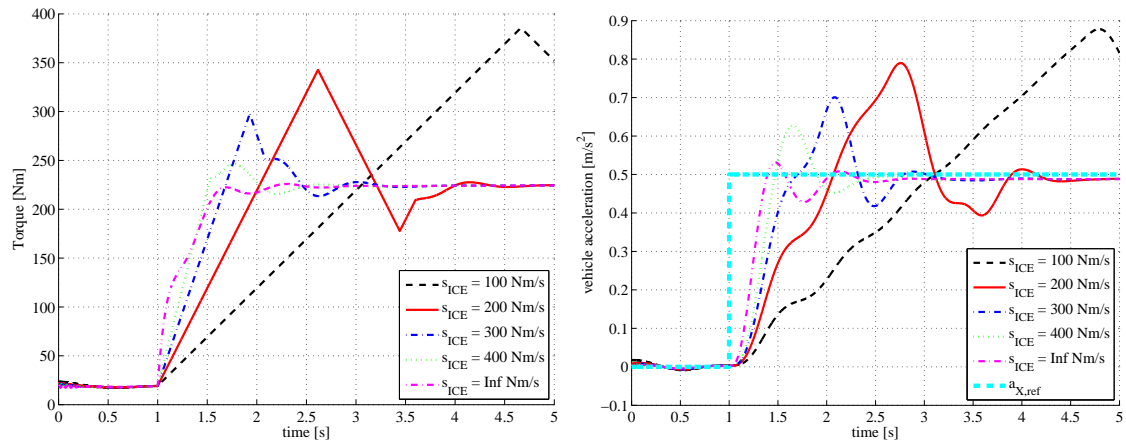
### ‘Hybrid’ operating mode with EM saturation

When the amplitude of the requested vehicle acceleration step becomes too large, or when the slope of the engine torque is too small, the power limitation of the electric actuator intervenes, thus determining an inevitable performance deterioration. Nevertheless, the closed loop control is able to mitigate the driver discomfort caused by the shuffle vibrations if compared with the engine only scenario.

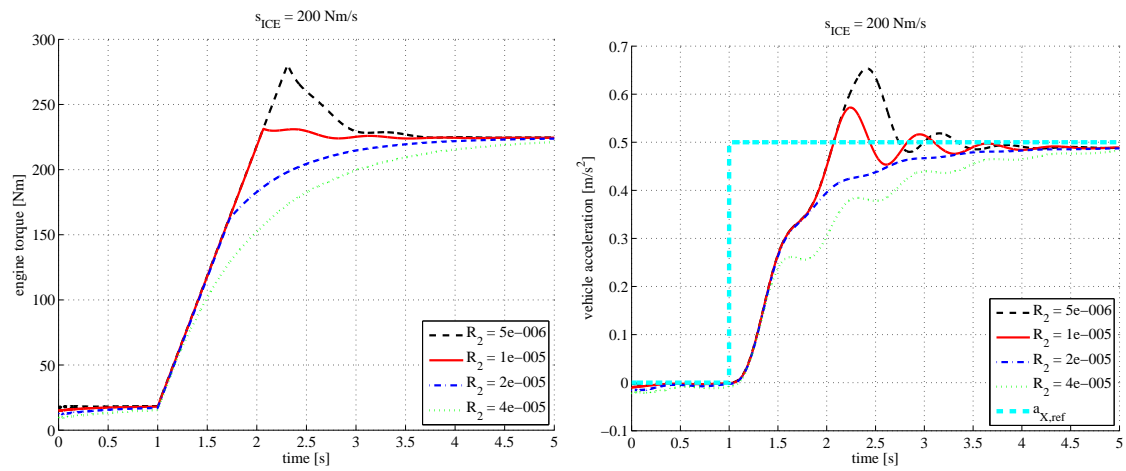
The effect of electric motor saturation is here evaluated, considering the closed loop response to step changes in the reference vehicle acceleration.

Figure 17 shows the maximum and minimum steady-state values of both the actuators; thus, it is possible to identify the electric motor saturation condition and its effect on vehicle performance. The last two tested values of acceleration, i.e.  $1.25$  and  $1.5 \text{ m/s}^2$ , involve a saturation of the





**Figure 12:** effect of the engine torque rate limitation on closed loop control of vehicle acceleration for a given control calibration ( $[R_2] = 10^{-6}$ ) in engine only mode: on the left the actual engine torque, on the right the resulting vehicle acceleration together with the set point profile



**Figure 13:** effect of different calibrations of the closed-loop control for a given maximum engine torque slope (200 Nm/s) in engine only mode: on the left the actual engine torque, on the right the resulting vehicle acceleration together with the set point profile

electric motor. As a consequence, the acceleration, visible in the right part of Fig.16, initially grows almost linearly, as imposed by the maximum engine slope (in the simulation 400 Nm/s); then it keeps constant, after the engine has reached its steady state value. For high reference accelerations, the electric motor cannot completely satisfy the total torque demanded by the control system, but the results show small acceleration oscillations and pretty fast transients. Table 1 summarises the maximum vehicle jerk obtained during tip-in tests using the engine-only open-loop mode (without torque rate limitation) and hybrid closed-loop mode: it is evident that even in saturation conditions the maximum jerk remains lower than in the open-loop case. Consequently, it can be concluded that the proposed control strategy guarantees satisfactory performances also in saturation conditions.

acceleration [m/s <sup>2</sup> ]	OL jerk [m/s <sup>3</sup> ]	CL jerk [m/s <sup>3</sup> ] no saturation	CL jerk [m/s <sup>3</sup> ] saturation
0.5	7.9	1.9	-
0.8	10.9	2.8	-
1.3	16.6	-	4.6
1.5	19.7	-	5.5

**Table 1:** Maximum jerk during tip-in tests for different final accelerations: comparison between open and closed loop control

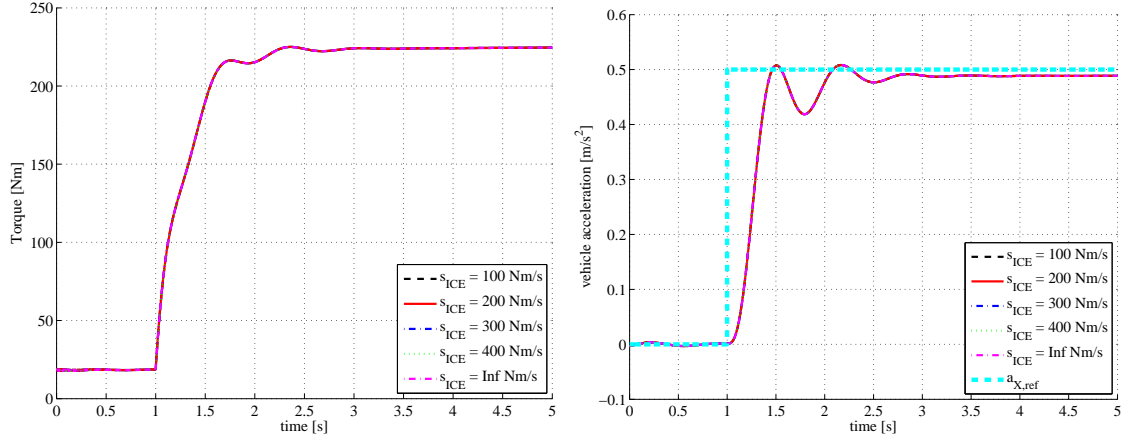


Figure 14: total torque and vehicle acceleration in hybrid operational mode

#### 4.5 Tip-in tip-out with active damping of drivetrain oscillations

Starting from the torque requested by the driver  $T_{dr}$ , a reference acceleration  $a_{x,ref}$  is computed. The function  $fv$  correlating the two quantities ( $fv$  block in the block diagram of Fig.8), can be obtained by reducing the system to a single degree of freedom, according to the following hypotheses:

- the transmission and driveline components are supposed infinitely stiff
- the rear wheels slip is neglected
- the tyre response is assumed instantaneous (null relaxation length)

$$\ddot{v}_F = \eta_d \tau_d T_e - \frac{T_a(\omega_F) + T_i + T_{rF}(\omega_F) + T_{rR}(\omega_F)}{J_v + J_R + \eta_d \tau_d^2 J_e} \quad (32)$$

$$a_{x,ref} = R_w \ddot{v}_F = \eta_d \tau_d T_e - C_0 - C_2 \omega_F^2. \quad (33)$$

Therefore, eq.(32) and (33) give the vehicle acceleration that would arise if the transmission and driveline could be considered infinitely stiff. Under this hypothesis, the total input torque and acceleration are simply linked by a scale factor, without dynamic distortion. The gain depends linearly on the actual transmission gear ratio  $\tau_d$ , while the offset depends on the squared wheel speed  $\omega_F^2$ , as detailed in eq.(33), where  $C_0$  and  $C_2$  are introduced to group the constants. Then the acceleration is converted into a reference speed for the front wheels, the controlled state variable, so that the control loop can be closed.

The closed loop control system practically superposes a torque correction to the open loop driver request with the aim of reducing the driveline torsional oscillations.

A tip-in tip-out test has been simulated and the results are shown in Fig.18 and 19. The aim of the comparison is to highlight the benefits introduced by the adoption of the electric motor in enhancing the vehicle drivability. First of all, the response to ideal torque steps is reported in order to underline the slightly damped behaviour of the transmission. The second curve represented is relative to the engine only mode with a closed-loop control aiming at reducing the vibrations: the vehicle acceleration shows smooth transitions between the steady state values but relatively slow response, due to the torque slope saturation. Finally, the hybrid mode presents faster response speed while maintaining a low level of vibrations. The electric motor supports the engine during transients, so that the engine can continue to work with slow torque gradients, thus reducing the associated transient emissions.

#### 4.6 Vehicle speed closed loop control

A last control structure, easily referable to the former ones, is here introduced. The control system behaves as a cruise control, thus trying to satisfy the speed changes requested by the driver. Again a fast and smooth response can be achieved by combining the electric motor to the engine. In this

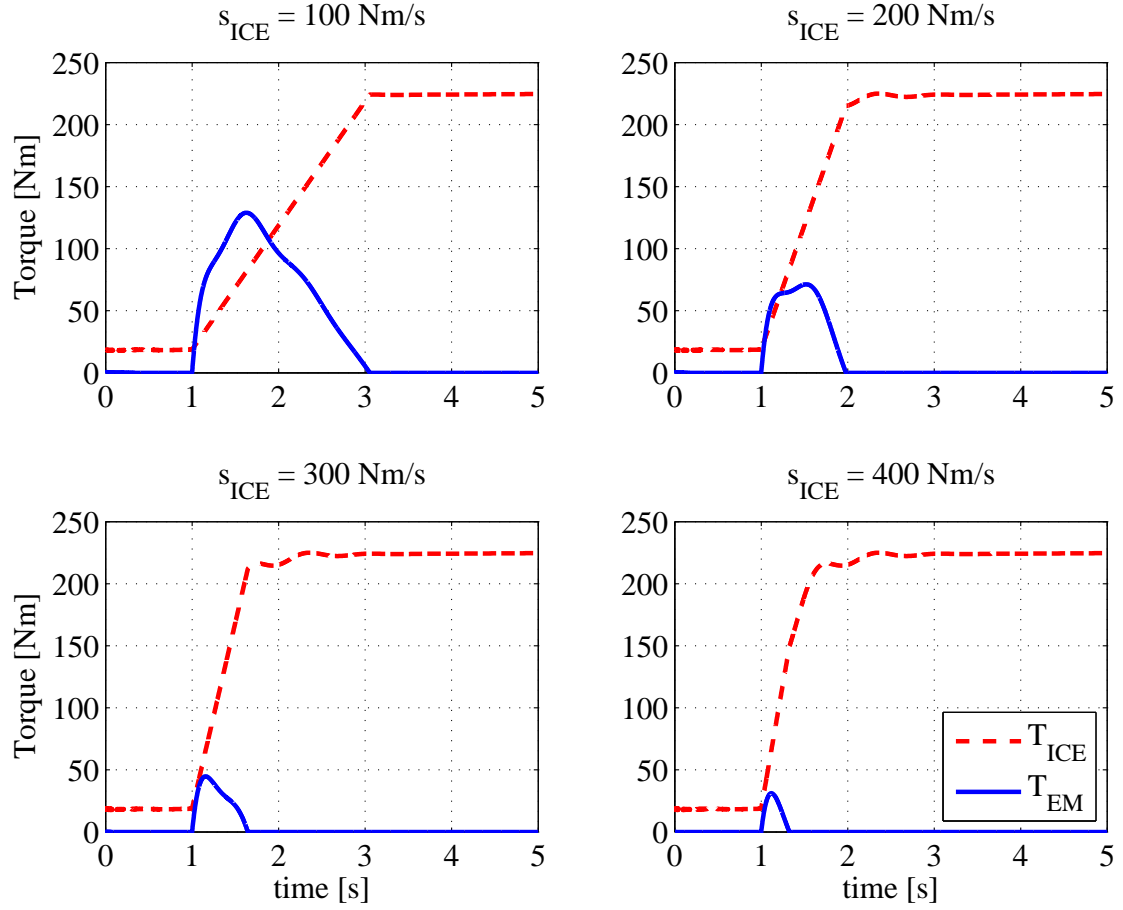


**Figure 15:** torque distribution between the actuators during a step response of the vehicle acceleration

case, since the tracking performance aims also at eliminating the steady state error, an integral action is introduced and the control law becomes:

$$v = K_I \int_0^t (\omega_{F,ref} - [C_F]\{x\}) dt - [K]\{\hat{x}\} \quad (34)$$

where  $K_I$  is the integral gain that can be tuned applying the LQR design methodology.

The ICE dynamic limits are compensated by the EM activation to cover the torque peaks request: the EM increases the dynamic response while reducing the oscillations.

$M_v$	16 ton	$R_w$	0.501 m	$L_t$	0.2 m
$\gamma$	0.4 [-]	$S_v$	7.6 m <sup>2</sup>	$D$	0.87 [-]
$J_e$	2.6 kgm <sup>2</sup>	$J_F$	3 kgm <sup>2</sup>	$J_R$	6 kgm <sup>2</sup>
$\tau_b$	1 [-]	$\tau_{IV}$	35.04 [-]	$\tau_{VIII}$	16.91 [-]
$P_{ICE}$	332 kW	$T_{ICE}$	2100 Nm	$k_s$	175 kNm/rad
$P_{EM}$	31 kW	$T_{EM}$	300 Nm	$C_t$	420 kN
$f$	$8 \cdot 10^{-3}$ [-]	$K$	$9.03 \cdot 10^{-6} \text{s}^2/\text{rad}^2$		

**Table 2:** Truck data

## 5 Conclusion

This paper discusses the model and control of a mild-hybrid electric truck, with a BAS architecture, aiming at improving the vehicle drivability and reducing the emissions of the diesel engine due to fast load changes.

In particular, the main results can be summarised as follows:

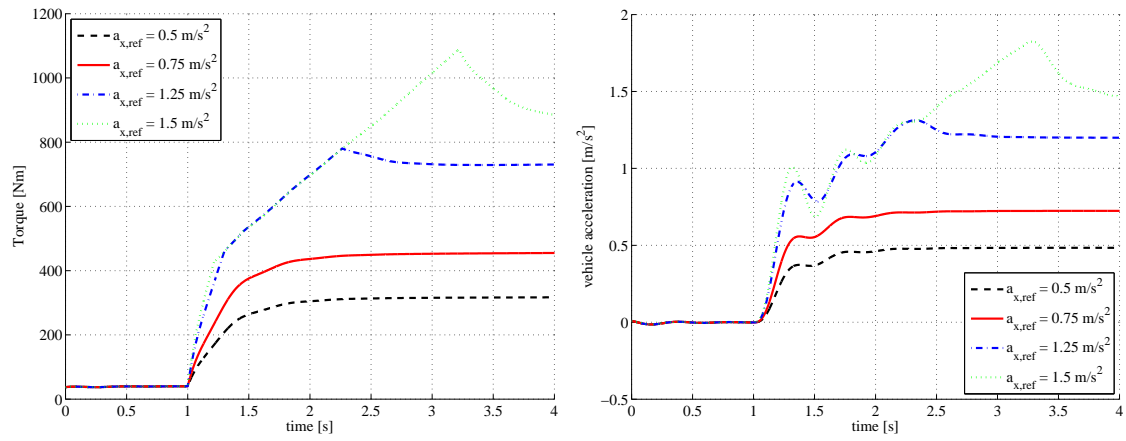


**Figure 16:** effect of actuators saturations: on the left the total torque  $T_e$ , on the right the vehicle acceleration (simulation settings: 8<sup>th</sup> gear, initial speed 10 km/h,  $s_{ICE} = 400 \text{ Nm/s}$ )

- at least a 5-state linearised model must be used to characterise the truck behaviour during tip-in/tip-out manoeuvres; the pure rolling motion hypothesis for the drive wheels causes a raw estimation of both resonance frequency and damping;
- the linearisation of the truck model, introduced in the SS5 model, does not significantly affect the vehicle response in terms of longitudinal acceleration; greater differences have been highlighted in tyre slip especially during fast transients;
- the differences between SS3 and SS5 highlighted in open loop are less evident in closed loop: the three state controller is able to provide the required performance for the closed loop control system and, moreover, the calibration made on the SS3 linear model can be extended to control the nonlinear model with a fairly accurate approximation of the achievable response;
- the effect on drivability of the engine torque slope for a pure thermal vehicle has been analysed both in open-loop and closed-loop: the slope reduction of the engine torque is an effective way to reduce oscillations in open-loop; on the contrary, in closed-loop control, the slower response of the actuator leads to a degradation of the dynamic performance;
- the effect of different calibrations of the closed-loop control has been simulated: different torque gradients require different control calibrations to achieve the best dynamic performance;
- if the rise time is not a critical design constraint, a first order low-pass filter can be applied on the engine torque to obtain a slow but smooth vehicle acceleration profile;
- a high dynamic electric motor can be effectively used, in combination with the thermal engine, to increase the promptness of the vehicle response and concurrently damp the torsional vibrations;
- the proposed control strategy guarantees that the electric motor, within its saturation limits, can completely overcome the dynamic limit of the IC engine and cope the ideal performance achievable with the considered driveline; satisfactory performances are obtained also in saturation conditions;
- an engine emission control strategy that smooths the high rate of engine load changes, with the aim of minimising the emission formation (NOx and soot), can be easily implemented in this hybrid architecture, considering that the electric motor is able to cover the impulsive torque requested by the drivability controller;
- the hybrid architecture together with the proposed control schemes constitutes an effective way to establish a trade-off between emissions and dynamic performance.

## References

Anderson, B.D.O., Moore, J.B. (1990) *Optimal Control: Linear Quadratic Methods*, Prentice Hall, Upper Saddle River (USA).

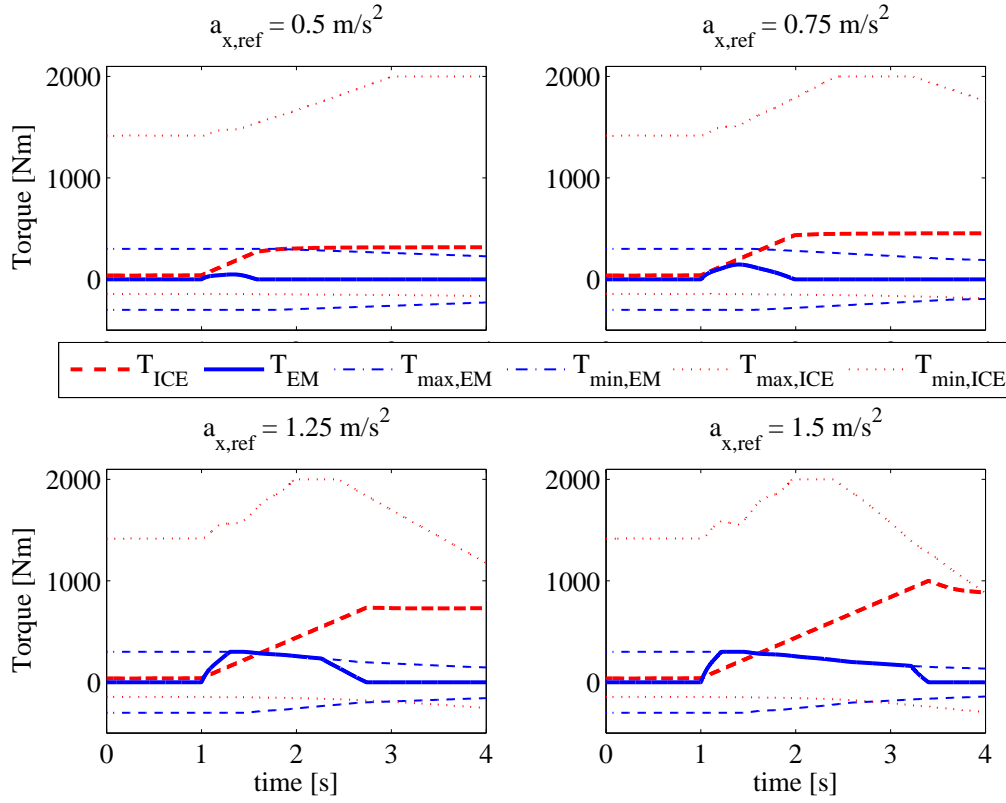


**Figure 17:** effect of actuators saturations: control effort distribution between the actuators

- Auerbach, M., Ruf, M., Bargende, M., Reuss, H. et al. (2011) ‘Potentials of Phlegmatization in Diesel Hybrid Electric Vehicles’, *SAE Technical Paper 2011-37-0018*, doi:10.4271/2011-37-0018.
- Bartram, M., Mavros, G. and Biggs, S. (2010) ‘A study on the effect of road friction on driveline vibrations’, *Proceedings of the Institution of Mechanical Engineers, Part K: Journal of Multi-body Dynamics*, 224, pp.321–340, doi: 10.1243/14644193JMBD266.
- Baumann, J., Torkzadeh, D.D., Ramstein, A., Kiencke, U. and Schlegl, T. (2006) ‘Model-based predictive anti-jerk control’, *Control Engineering Practice*, 14, pp.259–266, doi: 10.1016/j.conengprac.2005.03.026.
- Berriri, M., Chevrel, P. and Lefebvre, D. (2008) ‘Active damping of automotive powertrain oscillations by a partial torque compensator’, *Control Engineering Practice*, 16, pp.874–883, doi: 10.1016/j.conengprac.2007.10.010.

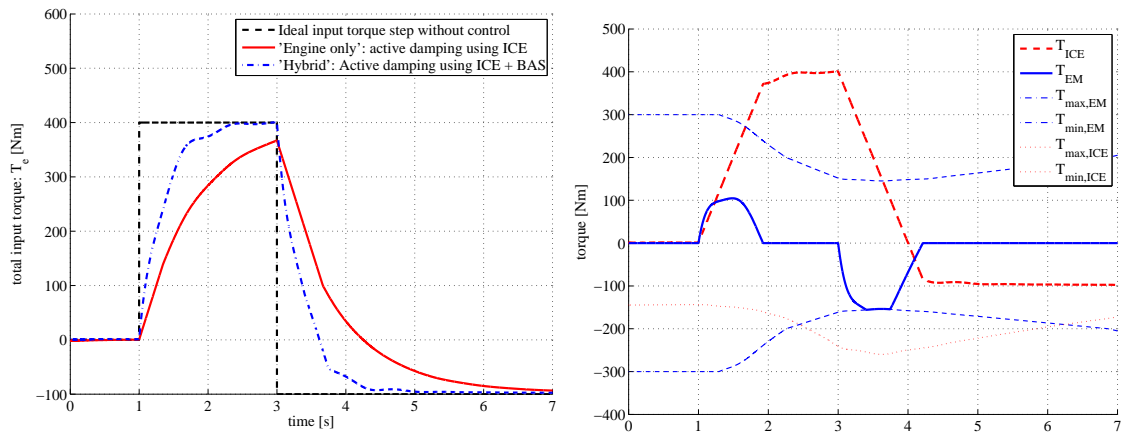


**Figure 18:** active damping of driveline vibrations: on the left the total torque  $T_e$ , on the right the torque distribution between the actuators in hybrid mode (simulation settings: 4<sup>th</sup> gear, initial speed 5 km/h,  $s_{ICE} = 400$  Nm/s)

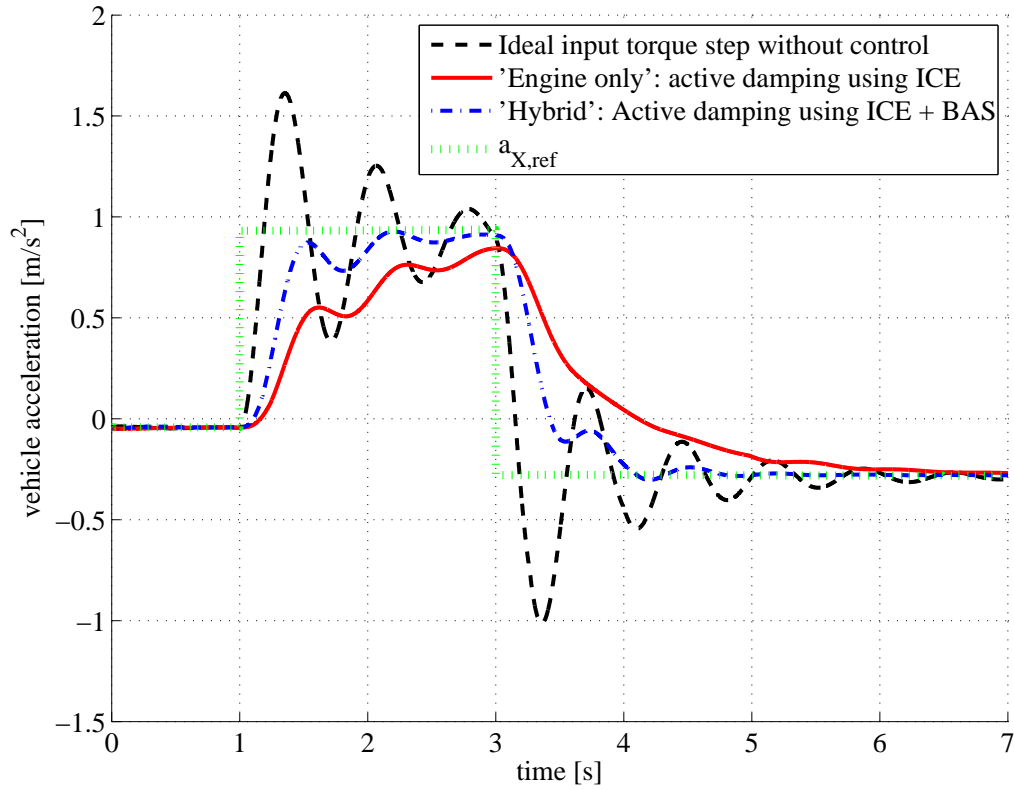


**Figure 19:** active damping of the driveline vibrations: vehicle acceleration

- Canudas-de-Wit, C., Tsiotras, P., Velenis, E., Basset, M. and Gissinger, G. (2003) 'Dynamic Friction Models for Road/ tyre Longitudinal Interaction', *Vehicle System Dynamics*, 39 (3), pp. 189–226, doi: 10.1076/vesd.39.3.189.14152.
- Diversi, R., Guidorzi, R. and Soverini, U. (2005) 'Kalman filtering in extended noise environments', *IEEE Transactions on Automatic Control*, 50, pp.1396–1402.
- Dolcini, P.J., Canudas-de-Wit, C. and Béchart H. (2010) *Dry Clutch Control for Automotive Applications*, Springer, Berlin.
- Dorf, R.C. and Bishop, R.H. (2008) *Modern Control Systems*, Prentice Hall, Upper Saddle River.
- Farshidianfar, A., Ebrahimi, M. and Bartlett H. (2001) 'Hybrid modelling and simulation of the torsional vibration of vehicle driveline systems', *Proceedings of the Institution of Mechanical Engineers, Part D: J. of Automobile Engineering*, pp.215–217, doi: 10.1243/0954407011525593.
- Fredriksson, J. (2006) 'Improved Driveability of a Hybrid Electric Vehicle Using Powertrain Control', *Int. J. Alternative Propulsion*, 1 (1) , pp.97–111.
- Guzzomi, A.L., Sharman, A. and Stone, B.J. (2010) 'Some torsional stiffness and damping characteristics of a small pneumatic tyre and the implications for powertrain dynamics', *Proceedings of the Institution of Mechanical Engineers, Part D: J. of Automobile Engineering*, pp.224–229, doi: 10.1243/09544070JAUTO1194.
- Hagena, J. R., Filipi, Z. S. and Assanis, D.N., (2006), 'Transient Diesel Emissions: Analysis of Engine Operation During a Tip-In', SAE Technical Paper 2006-01-1151, doi:10.4271/2006-01-1151.
- Härkegård, O. (2003) *Backstepping and Control Allocation with Applications to Flight Control*, PhD. Thesis, Linköping, Sweden.
- Koprubasi, K. (2008) *Modeling and Control of a Hybrid-Electric Vehicle for Drivability and Fuel Economy Improvements*, PhD. Thesis, Ohio State University, Ohio (USA).
- Ito, Y., Tomura, S. and Moriya, K. (2007) 'Development of Vibration Reduction Motor Control for Hybrid Vehicles', *Industrial Electronics Society (IECON 2007), 33rd Annual Conference of the IEEE*, pp.516–521, doi: 10.1109/IECON.2007.4460237.

Pacejka, H.B. (2002) *Tyre and Vehicle Dynamics*, Butterworth, Oxford.

Rill, G. (2006), ‘First order tyre dynamics’, *III European Conf. on Computational Mechanics, Solids, Structures and Coupled Problems in Engineering*, Lisbon, Portugal.

## Appendix A

### subscripts

$a$	aerodynamic
$d$	driveline
$e$	equivalent total motor: internal combustion engine plus electric motor
$i$	road inclination
$p$	primary shaft
$r$	rolling resistance
$s$	drive shaft
$t$	tyre
$v$	vehicle
$w$	wheel
$x$	longitudinal axis
$z$	vertical axis
EM	electric motor
$F$	front axle
ICE	internal combustion engine
$R$	rear axle
0	equilibrium condition (for linearisation)

### superscripts

*	linearised force/torque
---	-------------------------

### symbols

$\alpha$	road longitudinal angle
$\beta$	viscous damping
$\gamma$	static load distribution on the front axle
$\delta$	delay due to the tyre relaxation length
$\eta$	efficiency
$\vartheta$	shaft angular position
$\rho$	air density
$\sigma$	longitudinal tyre slip
$\tau_b$	belt transmission ratio $\omega_{EM}/\omega_{ICE}$
$\tau_d$	overall transmission ratio $\omega_p/\omega_s$
$\omega = \dot{\vartheta}$	shaft speed
$f$	constant coefficient of the rolling resistance
$g$	gravity acceleration
$k$	stiffness
$s$	torque rate limit
$u$	input vector
$v$	input signal (SI system)
$C_t$	tyre longitudinal slip stiffness
$D$	aerodynamic drag coefficient
$J$	mass moment of inertia
$K$	quadratic coefficient of the rolling resistance
$L$	relaxation length
$M$	vehicle mass
$N$	force
$P$	power
$[R_1], [R_2]$	LQR weight matrices
$R_w$	wheel radius
$S_v$	vehicle cross area/surface
$T$	torque
$V$	vehicle speed

## Appendix B

### Linearization of the equations of motion

Taylor expansion leads to

$$\tilde{T}_t = \frac{C_t R_w}{\dot{\vartheta}_{R0}} \left( \dot{\vartheta}_R - \frac{\dot{\vartheta}_{F0}}{\dot{\vartheta}_{R0}} \dot{\vartheta}_F \right) + \frac{C_t R_w}{\dot{\vartheta}_{R0}} \frac{\dot{\vartheta}_{R0} - \dot{\vartheta}_{F0}}{\dot{\vartheta}_{R0}} \quad (35)$$

let assume that in steady state conditions the angular speed of the rear axle is equal to the velocity of the front wheels, i.e.,  $\dot{\vartheta}_{R0} = \dot{\vartheta}_{F0}$ ; then it yields:

$$\tilde{T}_t = \beta_t (\dot{\vartheta}_R - \dot{\vartheta}_F) \quad (36)$$

where  $\beta_t$  is

$$\beta_t = \frac{C_t R_w}{\dot{\vartheta}_{R0}} \quad (37)$$

The linearised expression of the resistant torque due to the aerodynamic drag is:

$$T_a^* = -\frac{1}{2} \rho S_v D R_w^3 \dot{\vartheta}_{F0}^2 + \rho S_v D R_w^3 \dot{\vartheta}_{F0} \dot{\vartheta}_F \quad (38)$$

For the rolling resistance, Taylor expansion in the neighbourhood of a steady state condition results

front axle

$$T_{rF}^* = \gamma N_z R_w (f - K \dot{\vartheta}_{F0}^2) + 2\gamma N_z K R_w \dot{\vartheta}_{F0} \dot{\vartheta}_F \quad (39)$$

rear axle

$$T_{rR}^* = (1 - \gamma) N_z R_w (f - K \dot{\vartheta}_{R0}^2) + 2(1 - \gamma) N_z K R_w \dot{\vartheta}_{R0} \dot{\vartheta}_R \quad (40)$$

In order to express the system in the state space, let introduce the following state variables: drive shaft relative angular displacement  $x_1$ , rear wheels angular speed  $x_2$ , primary shaft angular speed  $x_3$ , equivalent rotational vehicle speed  $x_4$  and delayed tyre/road torque  $x_5$ , i.e.:

$$x_1 = \frac{\vartheta_p}{\tau_d} - \vartheta_R \quad (41)$$

$$x_2 = \dot{\vartheta}_R \quad (42)$$

$$x_3 = \dot{\vartheta}_p \quad (43)$$

$$x_4 = \dot{\vartheta}_F \quad (44)$$

$$x_5 = T_t \quad (45)$$

The linearized dynamic equations are:

$$\dot{x}_1 = -x_2 + \frac{x_3}{\tau_d} \quad (46)$$

$$\begin{aligned} \dot{x}_2 = & \frac{k_s}{J_R} x_1 - \frac{\beta_s + 2(1 - \gamma) Mg \cos \alpha K R_w \dot{\vartheta}_{R0}}{J_R} x_2 + \frac{\beta_s}{J_R \tau_d} x_3 - \frac{1}{J_R} x_5 + \\ & - \frac{(1 - \gamma) Mg \cos \alpha R_w (f - K \dot{\vartheta}_{R0}^2)}{J_R} \end{aligned} \quad (47)$$

$$\dot{x}_3 = -\frac{k_s}{\eta_d \tau_d J_e} x_1 + \frac{\beta_s}{\eta_d \tau_d J_e} x_2 - \frac{\beta_s}{\eta_d \tau_d^2 J_e} x_3 + \frac{T_{ICE} + \tau_b T_{EM}}{J_e} \quad (48)$$

$$\begin{aligned} \dot{x}_4 = & -\frac{\rho S_v D R_w^3 \dot{\vartheta}_{F0} + 2\gamma Mg \cos \alpha K R_w \dot{\vartheta}_{F0}}{J_v} x_4 + \frac{1}{J_v} x_5 + \\ & - \frac{Mg \sin \alpha R_w - \frac{1}{2} \rho S_v D R_w^3 \dot{\vartheta}_{F0}^2 + \gamma Mg \cos \alpha R_w (f - K \dot{\vartheta}_{F0}^2)}{J_v} \end{aligned} \quad (49)$$

$$\dot{x}_5 = \frac{\beta_t}{\delta} x_2 - \frac{\beta_t}{\delta} x_4 - \frac{1}{\delta} x_5 \quad (50)$$



In matrix form it holds:

$$\{\dot{x}\} = [A]\{x\} + [B]\{u\} + [H] \quad (51)$$

where:

$$\{x\} = \begin{bmatrix} x_1 \\ x_2 \\ x_3 \\ x_4 \\ x_5 \end{bmatrix} = \begin{bmatrix} \vartheta_p/\tau_d - \vartheta_R \\ \dot{\vartheta}_R \\ \dot{\vartheta}_p \\ \dot{\vartheta}_F \\ T_t \end{bmatrix} \quad (52)$$

$$\{u\} = \begin{bmatrix} u_1 \\ u_2 \end{bmatrix} = \begin{bmatrix} T_{\text{ICE}} \\ T_{\text{EM}} \end{bmatrix} \quad (53)$$

$$[A] = \begin{bmatrix} 0 & -1 & 1/\tau_d & 0 & 0 \\ \frac{k_s}{J_R} & -\frac{\beta_s + 2(1-\gamma)Mg \cos \alpha K R_w \dot{\vartheta}_{R0}}{J_R} & \frac{\beta_s}{\tau_d J_R} & 0 & -\frac{1}{J_R} \\ -\frac{k_s}{\eta_d \tau_d J_e} & \frac{\beta_s}{\eta_d \tau_d J_e} & -\frac{\beta_s}{\eta_d \tau_d^2 J_e} & 0 & 0 \\ 0 & 0 & 0 & -\frac{\rho S_v D R_w^3 \dot{\vartheta}_{F0} + 2\gamma Mg \cos \alpha K R_w \dot{\vartheta}_{F0}}{J_v} & \frac{1}{J_v} \\ 0 & \frac{\beta_t}{\delta} & 0 & -\frac{\beta_t}{\delta} & -\frac{1}{\delta} \end{bmatrix} \quad (54)$$

$$[B] = \begin{bmatrix} 0 & 0 \\ 0 & 0 \\ \frac{1}{J_e} & \frac{\tau_b}{J_e} \\ 0 & 0 \\ 0 & 0 \end{bmatrix} \quad (55)$$

$$[H] = \begin{bmatrix} 0 \\ -\frac{(1-\gamma)Mg \cos \alpha R_w (f - K \dot{\vartheta}_{R0}^2)}{J_R} \\ 0 \\ -\frac{Mg \sin \alpha R_w - \frac{1}{2}\rho S_v D R_w^3 \dot{\vartheta}_{F0}^2 + \gamma Mg \cos \alpha R_w (f - K \dot{\vartheta}_{F0}^2)}{J_v} \\ 0 \end{bmatrix} \quad (56)$$